International Journal of Solids and Structures 90 (2016) 144–152

Contents lists available at ScienceDirect

International Journal of Solids and Structures

journal homepage: www.elsevier.com/locate/ijsolstr

Mesh refinement schemes for the concurrent atomistic-continuum method

Shuozhi Xu[a,*], Liming Xiong[b], Qian Deng[c], David L. McDowell[a,d]

[a] GWW School of Mechanical Engineering, Georgia Institute of Technology, Atlanta, GA 30332-0405, USA
[b] Department of Aerospace Engineering, Iowa State University, Ames, IA 50011, USA
[c] School of Aerospace, Xi'an Jiaotong University, Xi'an, Shaanxi 710049, PR China
[d] School of Materials Science and Engineering, Georgia Institute of Technology, Atlanta, GA 30332-0245, USA

ARTICLE INFO

Article history:
Received 30 August 2015
Revised 27 March 2016
Available online 13 April 2016

Keywords:
Concurrent atomistic-continuum method
Brittle-to-ductile transition
Mesh refinement
Dislocation migration

ABSTRACT

Most concurrent multiscale methods that employ domain decomposition divide the simulation domain into atomistic and continuum subdomains such that nanoscale defects are described at atomistic resolution while a continuum treatment is employed elsewhere. An example is the concurrent atomistic-continuum (CAC) method. While dislocations can nucleate and migrate in the continuum domain in CAC, they are restricted to prescribed slip planes along interelement boundaries. In this paper, we extend the original CAC method by implementing mesh refinement schemes in a straightforward manner to accommodate a 3-D dislocation network and curved dislocation migration. CAC simulation results are validated by comparing to their equivalent fully atomistic simulations. Augmented with an adaptive mesh refinement scheme, a brittle-to-ductile transition in dynamic fracture response of single crystalline FCC Cu is accurately predicted using CAC simulations. Differing from most multiscale methods, the complexity of the geometric topologies during mesh refinement is avoided in this approach because CAC does not require interelement compatibility. The extended CAC method is expected to apply in multiscale modeling of more complex dislocation activities in crystalline materials up to μm scale.

1. Introduction

Most modelling and simulation in mechanics of materials involve numerical discretization, either temporal or spatial (Belytschko et al., 2014). For example, the derivative of a single variable function can be approximated by a difference quotient; an integral can be thought as an infinite sum of rectangles of infinitesimal width (Chapra and Canale, 2009). In continuum mechanics, the most commonly employed approach for spatial discretization is the finite element method (FEM), which converts partial differential equations into variational integral equations to find approximate solutions to boundary value problems (Zienkiewicz et al., 2013). In so doing, the continuum domain is partitioned into a number of smaller subdomains, over each of which the governing equations can be solved more easily. The discretization error of FEM is thus determined by whether the domain is well partitioned and whether each subdomain, i.e., an element, is correctly solved. This is analogous to approximating a curve by connecting many tiny straight segments: shorter segments should be employed where the target curve has a high curvature.

The employment of continuous subdomains with varying sizes in spatial discretization becomes problematic in the presence of nanoscale defects; in such cases, the continuum approximation begins to break down. Atomistic simulations such as molecular dynamics (MD) and molecular statics (MS) are more suitable for modeling defects such as nanoscale cracks or dislocations. In these non-local particle methods, spatial discretization is not necessary and defects are naturally allowed. However, the high computational cost of atomistic simulations makes their application to larger domains impractical. Thus, numerous concurrent multiscale methods have been developed to connect the continuum domain with the atomistic one when both are updated concurrently in time (Rudd and Broughton, 2000).

In most multiscale methods, atomistic resolution is usually retained where a large deformation gradient exists and/or explicit description of nanoscale phenomena is essential; otherwise, the continuum treatment is employed. While the atomistic domain is considered to render the "exact" solution within the uncertainty of the interatomic potential, it should be applied only in the neighborhood of area of interest, e.g., defects, to reduce the number of

* Corresponding author. Tel.: +14043767572.
E-mail address: shuozhixu@gatech.edu (S. Xu).

http://dx.doi.org/10.1016/j.ijsolstr.2016.03.030
0020-7683/

degrees of freedom in the system (Tadmor and Miller, 2012). Such a pre-partitioned domain works well when the spatial distribution of defects is invariant or when defects migrate along prescribed paths. In a more realistic case, however, the locations and migration paths of defects are difficult to predict *a priori*. Unlike in FEM where all subdomains are of continuum character, a concurrent multiscale simulation concerns subdomains of both continuum nature and discrete atoms. This suggests that a larger numerical error could occur as the system evolves if the continuum domain, which cannot explicitly model nanoscale defects, is not converted to discrete atoms, as necessary. Therefore, it is crucial and natural for most concurrent multiscale methods, especially in time dependent dynamic problems, to re-partition the domain down to the atomic scale on-the-fly, a process called adaptive remeshing in FEM. Concurrent multiscale methods augmented with mesh refinement, either adaptive or non-adaptive, are referred to as mesh refining multiscale methods in this paper.

In FEM, there are three remeshing techniques: (1) reducing or increasing the mesh size (*h*-refinement), (2) varying the polynomial degree of the interpolation basis (*p*-refinement), and (3) relocating or moving a mesh (*r*-refinement), where the refinement criterion is often expressed in form of the relative error in total strain energy (Zienkiewicz et al., 2013). A combination of these procedures, e.g., *hp*-refinement, is also widely employed. In adaptive multiscale methods, similar procedures can be adopted to decide whether a larger atomistic domain and/or a higher order continuum domain become necessary. To our knowledge, most adaptive multiscale methods employ *h*-refinement. The key is to maintain the atomic-scale resolution around the defects, e.g., dislocations, in a subdomain such that it encompasses the highly nonlinear and nonlocal behavior through mesh refinement.

In the quasicontinuum (QC) method (Tadmor et al., 1996), for example, a dislocation nucleated in the atomistic domain cannot migrate into the continuum domain, unless it is locally refined to atomic scale to render the dislocation. Several adaptive QC methods have been proposed, where elements are refined to distributions of atoms according to eigenvalues of the right stretch tensor (Shenoy et al., 1998), Green's strain (Park and Im, 2008), or a goal-oriented *a posteriori* error estimator (Arndt and Luskin, 2008). The same error estimator can also be used to remove unnecessary representative atoms (repatoms) from the mesh (Miller and Tadmor, 2002), similar to the *h*-refinement through which a collection of atoms is coarsened into a continuum. Moreover, the QC mesh can also be adaptively refined with *p*-refinement, e.g., using variable-node elements (Kwon et al., 2009).

In the coupled atomistic discrete dislocation (CADD) method (Shilkrot et al., 2004), dislocations can move from an atomistic to continuum domain where dislocations interact with each other through an elastic stress field dictated by continuum theory. In CADD, deformation near the atom/continuum interface can reach a value at which a larger size atomistic domain is needed, necessitating mesh refinement (Pavia and Curtin, 2015). Motivated by the key idea in CADD that the discontinuities due to dislocation-mediated slip in the continuum domain do not have to be retained at full atomistic resolution, Gracie and Belytschko (2009, 2011) developed an adaptive method combining the extended finite element method (XFEM) and the bridging domain method (BDM) to model moving dislocations. A crucial component of the adaptive XFEM-BDM framework is that the displacement discontinuities are specified through a step function across the active slip planes in continuum region by means of XFEM enrichments (Belytschko and Black, 1999; Belytschko et al., 2001; Moës et al., 1999). In adaptive XFEM-BDM, the mesh is refined and coarsened based on either of these two criteria: (1) the broken inter-atomic bonds and (2) the errors in atomic displacements associated with introducing a continuum field (Moseley et al., 2012).

In summary, most mesh refining multiscale methods for passing dislocations between atomistic and continuum domains can be classified into two types based on whether the dislocations are permitted in the continuum. The first type includes the QC-like methods, in which all elements in the continuum domain need to be refined locally to atomic scale fidelity to address dislocations. Consequently, the number of degrees of freedom scales with the defect volume, even with the aid of mesh coarsening. The second type includes the CADD-like methods, where the continuum domain describes lattice defects by either constitutive relations or lattice elasticity with dislocation field interactions, in the same way as in dislocation dynamics (DD), the cohesive zone method (CZM), or XFEM. Compared with methods of the first type, mesh refinement in the second type of method is less demanding. For example, dislocations exist in both DD and XFEM while cracks can be handled in both CZM and XFEM. Other types of discontinuities, such as point defects and complex dislocation junctions, may only be described accurately in the atomistic domain, and so mesh refinement is still necessary. For both types of mesh refining multiscale methods, one common issue is the geometric complexity during the mesh adaptation, due to either the interelement compatibility requirement in the first type of method or the heuristic dislocation passing/enrichment strategies between two domains in the second type of method.

In this paper, we extend the recently developed concurrent atomistic-continuum (CAC) method by implementing two mesh refinement schemes. In CAC, the same governing equations are employed in both atomistic and coarse-grained domains (Chen, 2006; 2009). In the atomistic domain, atoms are updated in the same way as in MD (for dynamic CAC) or MS (for quasistatic CAC); in the coarse-grained domain, possible separation or sliding between discontinuous elements accommodates brittle fracture (Deng et al., 2010) or dislocation glide (Xiong et al., 2011). As a result, unlike the first type of method, the elements in the coarse-grained domain in the vicinity of a dislocation do not have to be refined to the atomic scale. Additionally, there is no ghost force at the atomistic/coarse-grained domain interface, through which dislocations can pass smoothly, because (1) all atoms and nodes are nonlocal and (2) the same interatomic potential is employed in both domains as the only constitutive relation (Xu et al., 2015). This feature distinguishes CAC from the second type of method.

The governing equations for dynamic CAC come from the atomistic field theory (AFT), in which a crystalline material is viewed as a continuous collection of lattice points, each of which embeds a unit cell with a group of discrete atoms (Chen and Lee, 2005; Chen et al., 2011). For monoatomic crystalline materials, the governing equations reduce to the balance laws in classical continuum mechanics (Xiong et al., 2011). In the coarse-grained domain, a modified FEM method is employed to solve the mass and linear momentum balance equations by Gaussian quadrature (Xu et al., 2015). The similarity of the CAC method to FEM ensures its convergence and stability, and facilitates the mesh refinement procedure; for example, an *a posteriori* error estimator as in FEM can be introduced to assess the accuracy of the CAC method with mesh refinement themes. We refer the readers to some of our previous papers (Chen and Lee, 2003a, 2003b, 2003c; Xiong and Chen, 2009, 2012; Xiong et al., 2012b, 2014b, 2016; Xu et al., 2015, 2016) where details of the theoretical foundation, mathematical formulation, numerical implementation, and full capabilities of CAC are described.

In applying CAC to cubic crystals, dislocations in the coarse-grained domain migrate between discontinuous rhombohedral elements, all surfaces of which correspond to slip planes of the lattice, as shown in Fig. 1 of Xiong et al. (2011). CAC admits displacement discontinuity between elements because (1) non-local force/energy is used everywhere and (2) the governing equations can be written as an integral form without the spatial derivative. For crystalline

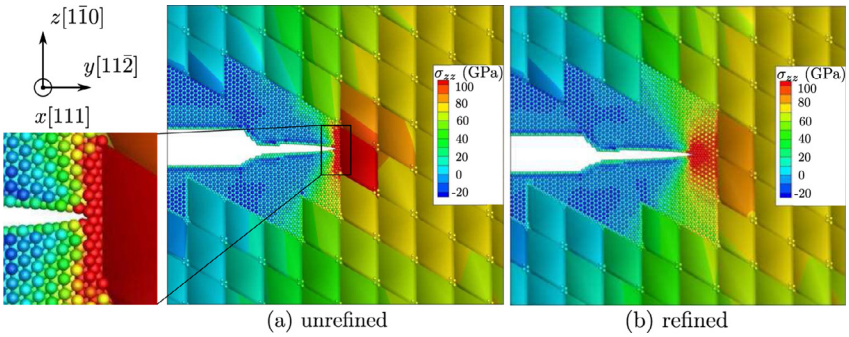

Fig. 1. (a) Without mesh refinement, the crack tip intersects the atomistic/coarse-grained domain interface at a location away from the interelement boundary, where a stress concentration occurs; the crack can neither propagate any further nor nucleate any dislocations. (b) With mesh refinement, the crack tip is again within the atomistic domain, and the stress concentration due to incompatibility of crack path is alleviated by restoring full atomistic degrees of freedom. Nodes and atoms are colored by tensile stress along the z-direction σ_{zz}. The lattice orientations are $x[111]$, $y[11\bar{2}]$, and $z[1\bar{1}0]$. (For interpretation of the references to color in this figure legend, the reader is referred to the web version of this article.)

metals in plastic deformation, dislocations can glide on 12 equivalent {111} ⟨110⟩ slip systems in face-centered cubic (FCC) lattice; in a body-centered cubic (BCC) system, possible slip systems include 12 sets of {110} ⟨111⟩ -type, 12 sets of {112} ⟨111⟩-type, and 24 sets of {123} ⟨111⟩-type. The rhombohedral elements in CAC, however, only permit dislocations in nine sets of {111} ⟨110⟩ and six sets of {110} ⟨111⟩ slip systems in FCC and BCC, respectively, thus confining other potential slip systems. Recently, a hybrid element was developed to exhibit all 12 slip systems in FCC system (Deng and Chen, 2013). However, the hybrid element is not employed in this paper due to its higher computational cost compared with a rhombohedral element of the same size: the former contains 122 integration points while the latter contains 64 integration points in the same first nearest neighbor element, solved by second-order Gaussian quadrature. Therefore, geometrically, only certain line/planar defects that are important for metal plasticity can be represented in the coarse-grained domain in the present CAC implementation, e.g., $\frac{1}{2}a_0\langle 110\rangle\{111\}$ full dislocations, $\frac{1}{6}a_0\langle 112\rangle\{111\}$ Shockley partial dislocations, intrinsic stacking faults, and dislocation intersection-induced jogs and kinks, where a_0 is the lattice parameter. Even for migration of these defects, it is required that their paths should be aligned with interelement boundaries. Defects that are not allowed directly in the coarse-grained domain include, but are not limited to, extended dislocation core structures, stacking fault tetrahedra, extrinsic stacking faults, superjogs, general grain boundaries, arbitrary cracks, and sessile dislocation locks such as Lomer, Hirth, and Lomer–Cottrell locks. Point defects and climb of a Frank partial dislocation, which is usually assisted by formation and migration of point defects, may be admitted in the coarse-grained domain but are not expected to be well described.

It is desirable to extend the CAC method by using mesh refinement schemes. For example, our previous CAC simulations of brittle fracture show that the coarse-grained domain with hybrid elements satisfactorily predicts local fracture behavior and average stress–strain relation comparable with fully resolved atomistic simulations with only 1.4% degrees of freedom of the latter (Deng and Chen, 2013). However, a ductile fracture process involving dislocations moving on multiple slip planes from the crack tip is restricted geometrically by element shape. For brittle fracture which mainly involves the rupture of atomic bonds (Bitzek et al., 2015), the coarse-grained domain works reasonably well because two neighboring elements are related by interatomic potentials; for ductile fracture, however, it is unlikely that the 3-D, time-varying, complex dislocation network, which is relevant to plastic response near a crack tip, can be captured using a limited number of slip planes. Also, note that in brittle fracture, the element shape and lattice orientation are carefully designed such that the element surfaces are also the cleavage planes; for arbitrary lattice orientations, brittle fracture may not be as well described using CAC without mesh refinement.

In the remainder of this paper, we first present the dynamic CAC framework furnished with two mesh refinement schemes in Section 2. Then, 3-D CAC simulations of brittle-to-ductile (BTD) transition in dynamic fracture and curved dislocation migration in FCC Cu are performed in Section 3 with the mesh refinement procedure. The extended CAC method is validated by comparing with equivalent fully atomistic simulations. The paper ends with a summary and discussion in Section 4.

2. Methodology

2.1. Dynamic CAC

In dynamic CAC, the Velocity Verlet form (Verlet, 1967) of the Brünger–Brooks–Karplus (BBK) integrator (Brünger et al., 1984) is employed in both atomistic and coarse-grained domains to update atoms and nodes, respectively. With all information at time t, the velocity is first advanced by half time step, i.e.,

$$\mathbf{v}\left(t+\frac{\Delta t}{2}\right)=\left(1-\gamma\frac{\Delta t}{2}\right)\mathbf{v}(t)+\frac{\Delta t}{2m}\mathbf{F}(t) \tag{1}$$

where Δt is the time step and γ is the damping coefficient. In the atomistic domain, m is the atomic mass and $\mathbf{F}$ is the atomic force; in the coarse-grained domain, m is the normalized lumped mass and $\mathbf{F}$ is the equivalent nodal force calculated by Gaussian quadrature (Xiong et al., 2011; Xu et al., 2015). The position is then propagated by

$$\mathbf{r}(t+\Delta t)=\mathbf{r}(\Delta t)+\mathbf{v}\left(t+\frac{\Delta t}{2}\right)\Delta t. \tag{2}$$

In the end, the velocity at time $(t+\Delta t)$ is obtained by

$$\mathbf{v}(t+\Delta t)=\frac{1}{1+\gamma\frac{\Delta t}{2}}\left[\mathbf{v}\left(t+\frac{\Delta t}{2}\right)+\frac{\Delta t}{2m}\mathbf{F}(t+\Delta t)\right]. \tag{3}$$

2.2. Adaptive mesh refinement scheme for dynamic fracture

In dynamic fracture, a crack can either propagate in a brittle manner or respond plastically by nucleating dislocations on multiple slip planes. A notched specimen of FCC Cu is employed for CAC simulations with atomistic resolution in the vicinity of crack and coarse elements employed elsewhere. As increasing remote tensile stress is applied to the system along the direction normal to the crack plane, atomic bonds at the crack tip are broken and

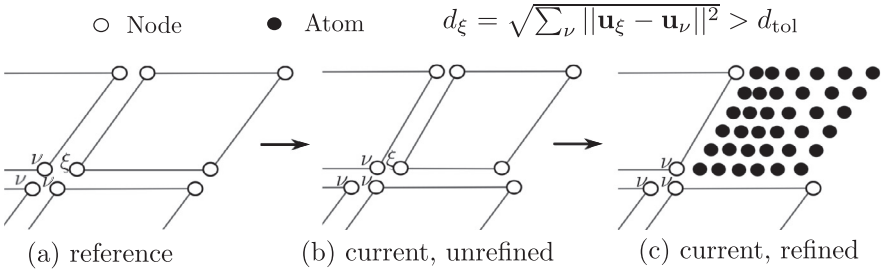

Fig. 2. 2-D illustration of adaptive mesh refinement procedure. (a) In the reference configuration, node ξ has three neighboring nodes ν; (b) periodically, the displacement of all four nodes are calculated by Eq. (4); (c) when $d^\xi > d_{\text{tol}}$, the element containing ξ is refined. The atoms in (c) are linearly interpolated from the nodes using their shape functions in undeformed configuration.

the crack extends. With lattice orientations of $x[111]$, $y[11\bar{2}]$, and $z[1\bar{1}0]$, we found that without mesh refinement, as the crack tip intersects the atomistic/coarse-grained domain interface away from an interelement boundary, a stress concentration occurs; the crack cannot propagate any further owing to the kinematic incompatibility with the original crack path, as shown in Fig. 1(a). If we refine the elements in front of the crack tip, the stress concentration is alleviated immediately as the crack tip is again within the atomistic domain, as shown in Fig. 1(b). These observations motivated development of an adaptive mesh refinement scheme to address dynamic fracture.

Unlike in FEM and most multiscale methods with a continuous mesh, neither displacement continuity nor strain compatibility between the discontinuous elements is required in CAC. Thus, the deformation gradient associated with the interior of a single element in CAC is generally too small to be used as an indicator in a remeshing criterion. Instead, we consider the magnitude of the discontinuity between elements and assign each node ξ a value d^ξ defined by

$$d^\xi = \sqrt{\sum_\nu ||\mathbf{u}^\xi - \mathbf{u}^\nu||^2} \tag{4}$$

where $\mathbf{u}$ is the nodal displacement vector and node ν is the neighbor of node ξ defined in the initial undeformed configuration. In 2-D and 3-D, each node has three and seven neighboring nodes located in different elements, respectively; a 2-D illustration is shown in Fig. 2. In undeformed or homogeneously deformed configurations, $d^\xi = 0$; in the presence of defects between elements, d^ξ becomes non zero. When any node ξ has a d^ξ exceeding a specified tolerance, d_{tol}, which is a function of a_0, an element is refined to full atomistic resolution by

$$\mathbf{R}^k = \boldsymbol{\phi}_{k\xi}\mathbf{x}^\xi \tag{5}$$

$$\dot{\mathbf{R}}^k = \boldsymbol{\phi}_{k\xi}\dot{\mathbf{x}}^\xi \tag{6}$$

where $\boldsymbol{\phi}_{k\xi}$ is the trilinear interpolation function, $\mathbf{x}^\xi$ ($\dot{\mathbf{x}}^\xi$) and $\mathbf{R}^k$ ($\dot{\mathbf{R}}^k$) are the positions (velocities) of node ξ and atom k, respectively. A flowchart of the CAC simulation algorithm with mesh refinement theme is illustrated in Fig. 3.

We note this is analogous to the use of deformation gradient in the QC approach to signal the need for adaptive remeshing. Compared with continuous FEM, the employment of discontinuous elements in CAC makes it more convenient to perform local mesh refinement without updating the global matrix thereafter or concerning the compatibility with its neighbors. The nature of the local formulation also promotes the parallelism of the algorithm as well as the workload rebalancing between processors during mesh refinement. Unlike in QC where the elements are constructed independently of the underlying lattice, the element boundaries in CAC are assumed to correspond to actual atomic sites, simplifying the procedure of locating the new atoms from refined elements. Note that the criterion defined in Eq. (4) can only be used to trigger remeshing of elements into full atomic resolution, but not vice versa, nor can it split a large element into multiple smaller ones.

We emphasize that for various mesh refinement criteria there always exists a tradeoff between accuracy, ease of implementation, and efficiency in selection. No matter which criterion is adopted, the goal of an adaptive mesh refinement approach is to detect and update subdomains which otherwise do not give accurate descriptions, so as to achieve a solution having a specified accuracy in an optimal fashion. By re-evaluating d^ξ periodically, an adaptive mesh refinement scheme will be employed to model BTD fracture in Section 3.1.

2.3. Mesh refinement scheme for dislocation migration

One major advantage of CAC is the allowance of dislocation nucleation and migration between discontinuous elements in the coarse-grained domain. However, CAC employs more nodes than other concurrent multiscale methods for the same number of elements. Therefore, a mesh refinement scheme for dislocation migration must take full advantage of the discontinuous elements by ensuring that a minimum number of elements are refined corresponding to dislocations that are not aligned with interelement boundaries. Possible scenarios in which mesh refinement is necessary for dislocation migration include, but are not limited to, (1) a dislocation migrating from atomistic to coarse-grained domain, as shown in Fig. 4(a), (2) from the coarse-grained domain with smaller elements to that with larger elements, as shown in Fig. 4(b), and (3) within the same coarse-grained domain with a uniform element size but for which elements are not aligned perfectly, as shown in Fig. 4(c).

An adaptive mesh refinement criterion based on Eq. (4) is useful for cases involving a complex dislocation network, e.g., 3-D dislocation nucleation under an indenter or from a void/precipitate/crack surface. However, this method refines all elements along the dislocation pathway, similar to the first type of mesh refining multiscale methods discussed in Section 1. Currently, a mesh refinement scheme is implemented in CAC based on manual remeshing to pass dislocations, as discussed in Section 3.2.

2.4. Parallel algorithms

From the perspective of parallelization, mesh refinement results in an immediate unbalance of workload between processors because the processors assigned with new atoms now have more tasks than that of the original elements. Parallel algorithms should be designed such that mesh refinement is accompanied by workload re-balancing.

Among the three parallel algorithms commonly employed in full atomistic simulations—atom decomposition (AD), force decom-

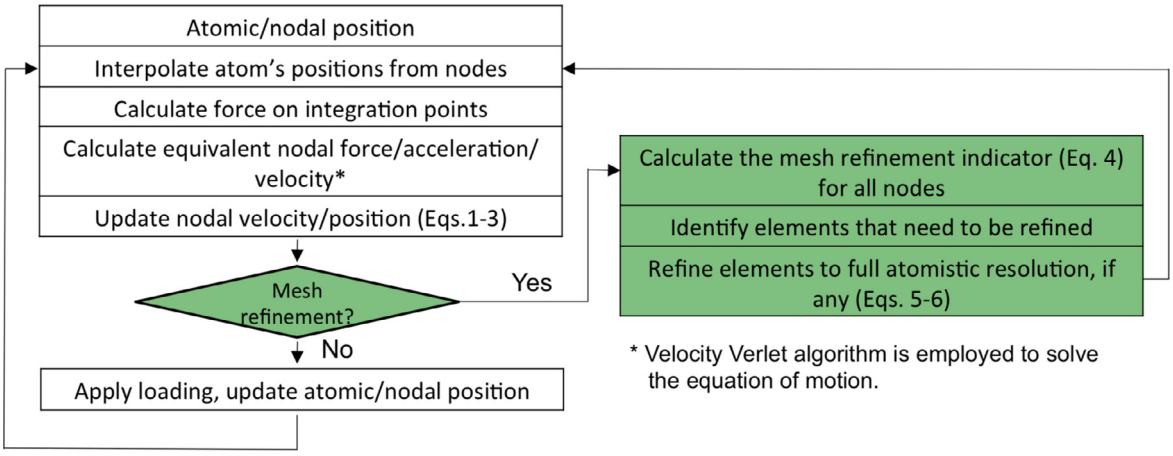

Fig. 3. CAC simulation algorithm with mesh refinement themes. The mesh refinement procedures are highlighted with light green, while the remaining procedures belong to the original CAC simulation theme. (For interpretation of the references to color in this figure legend, the reader is referred to the web version of this article.)

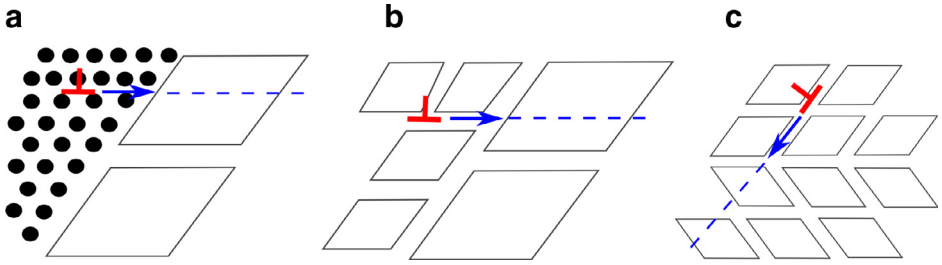

Fig. 4. Possible scenarios in which mesh refinement is necessary: (a) dislocation migration from atomistic to coarse-grained domain; (b) dislocation migration from the coarse-grained domain with smaller elements to that with larger elements; (c) dislocation migration within the same coarse-grained domain with a uniform element size but the elements are not aligned perfectly. Note that the situations encountered in a 3-D model can be much more complicated than those shown in these 2-D illustrations.

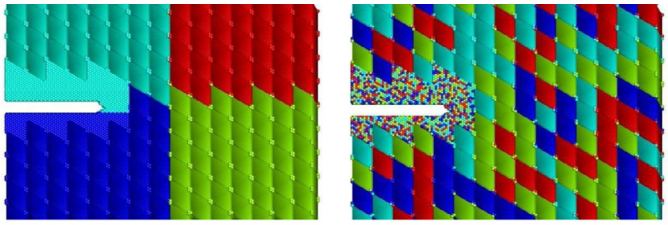

Fig. 5. Illustrations of two decomposition approaches in parallel CAC, where different processors are assigned domains with different colors: light blue, red, dark blue, and green. (a) Spatial decomposition with equally-sized domains for each processor; the processors assigned with light and dark blue domains have a heavier workload because they need to calculate the quantities of all atoms in the atomistic domain which has a higher density of interactions. (b) Force decomposition with perfectly balanced workload between processors. (For interpretation of the references to color in this figure legend, the reader is referred to the web version of this article.)

position (FD), and spatial decomposition (SD), SD yields the best scalability and the smallest communication overhead between processors (Plimpton, 1995). Unlike AD and FD, the workload of each processor in SD, which is proportional to the number of interactions, is not guaranteed to be the same. In CAC, the simulation cell has nonuniformly distributed integration points (in the coarse-grained domain) and atoms (in the atomistic domain), such that the workload is poorly balanced if we assign each processor an equally-sized cubic domain as in full atomistics, as shown in Fig. 5(a). This workload balance issue is not unique to CAC, but also encountered by other concurrent multiscale modeling methods (Pavia and Curtin, 2015). In CAC, two methods have been proposed to achieve a perfect or near perfect workload balance. The first method is the SD with unequally-sized domains, where the integration points and atoms are referred to as evaluation points; each processor domain is assigned approximately the same number of evaluation points (Xu et al., 2015). The second method is the FD, where the interactions between atomic pairs—either between the integration points and their neighbors in the coarse-grained domain or between the atoms and their neighbors in the atomistic domain—are evenly but spatially randomly assigned to each processor, as shown in Fig. 5(b). In this paper, both methods are applied, in which the workload is re-distributed between processors during mesh refinement. The AD approach is not considered due to its high communication overhead.

3. Computational models and simulation results

We next apply dynamic CAC to two problems: BTD dynamic fracture and curved dislocation migration, with two mesh refinement schemes employed, respectively. In both problems, no thermostat is employed in the atomistic domain, i.e., an NVE ensemble with a zero damping coefficient γ defined in Section 2.1; in the coarse-grained domain, $\gamma = 0.005$. Our recent predictions (Xiong et al., 2014b) showed that γ is not an artificial parameter *per se*, but rather a surrogate for the phonon drag on dislocation motion. The simulation results are visualized using Tecplot®, ParaView (Schroeder et al., 2006), and OVITO (Stukowski, 2010). The post-processing of the atomic structures in the coarse-grained domain is preformed after the atomic positions are linearly interpolated from the nodal positions. Some runs are completed using Blacklight and Comet on the NSF Extreme Science and Engineering Discovery Environment (XSEDE) (Towns et al., 2014).

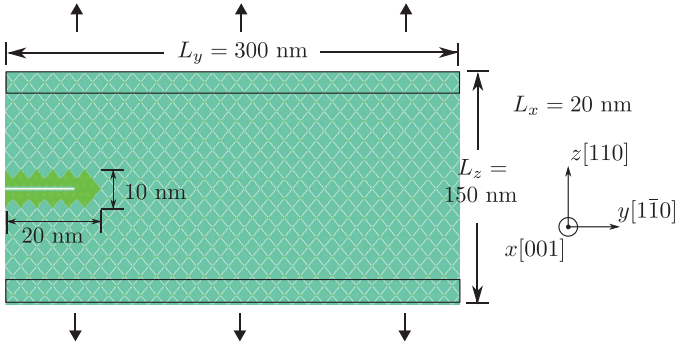

Fig. 6. Simulation cell for dynamic fracture of a FCC Cu specimen. An atomistic domain with 11,312 atoms is applied around the crack; elsewhere, 1414 elements with 8000 atoms per element are employed. Both top and bottom layers of elements are displaced uniformly, as shown to introduce a tensile displacement-controlled condition.

3.1. Brittle-to-ductile dynamic fracture

The fundamental mechanism of brittle versus ductile response of stressed crack tips is the competition between cleavage fracture by atomic decohesion and plastic deformation by dislocation nucleation and migration (Cheung and Yip, 1994; Xu, 2005). In particular, a BTD transition of crack behavior is favored by conditions of high temperature, low strain rate (Cheung and Yip, 1994), small specimen/grain size (Schulson and Barker, 1983), a large number of dislocation sources, high dislocation mobility (Gumbsch et al., 1998), and large stress/strain (Abraham et al., 1998).

The simulation cell for dynamic fracture is shown in Fig. 6. The notched specimen, which consists of FCC Cu atoms, has a size of 20 nm × 150 nm × 100 nm along x-, y-, and z-axes, respectively. Periodic boundary conditions (PBCs) are imposed along the x-direction, while boundaries normal to the y- and z-directions are traction free and fixed, respectively. We choose a model FCC crystal because it is inherently ductile and thus serves as a paradigm for plastic fracture (Abraham et al., 1997). The lattice orientations are $x[001]$, $y[1\bar{1}0]$, and $z[110]$. In total, there are 1414 elements with 8000 atoms per element. About 11,312 atoms are employed within a volume of 20 nm × 20 nm × 10 nm around the crack, which is created by deleting five layers of atoms normal to the z-direction. This corresponds to about 11.3 million atoms in an equivalent full atomistic model. Bonding for this model crystal is described by a simple two-body Lennard–Jones (LJ) potential, i.e.,

$$V(r) = 4\epsilon\left[\left(\frac{\sigma}{r}\right)^{12} - \left(\frac{\sigma}{r}\right)^{6}\right] \tag{7}$$

where r is the distance between atoms, $\epsilon = 0.167$, and $\sigma = 2.315$ (Kluge et al., 1990). The lattice parameter a_0 and cutoff distance are 3.616 and 5.38635 Å, respectively. We note that compared with a more realistic embedded-atom method (EAM) potential, the LJ potential overestimates the vacancy formation and migration energies (Daw and Baskes, 1984) and favors the BTD transition (Abraham, 1997); however, we emphasize that our intent in this paper is to establish the viability of adaptive mesh refinement procedure for CAC, instead of shedding light on improved understanding of dynamic fracture. The FD method is employed for parallelization.

Assigning zero initial velocities to all atoms and nodes, the simulation cell is subject to tension by relative vertical displacement δ of the top and bottom layers of elements. Two displacement rates are employed: $\dot{\delta} = 0.141$ m/s and 0.176 m/s, with $\Delta t = 5$ fs in both domains. As the simulation evolves, we evaluate d^{ξ} of all nodes at every time step, and refine an element if any of its node has a $d^{\xi} > (\sqrt{6}/12)a_0$. Note that the top and bottom layers of elements on which the displacement is directly applied are excluded from the mesh refinement procedure to avoid unnecessary computational cost. Dislocation activity at the crack tip is monitored every 10 time steps using the centrosymmetry parameter (Kelchner et al., 1998). Subject to a tensile displacement-controlled condition, the originally sharp crack tip in the fully resolved atomistic domain is initially blunted before the crack begins to propagate in a brittle manner without emitting any dislocations from the tip, as shown in Fig. 7. This marks the beginning of dynamic instability. As the crack speed increases, the energy at the crack tip accumulates. As a result, when the crack passes the middle region of the model, it responses plastically, where a "flower-of-loop" shape of dislocations are nucleated on multiple slip planes, as shown in Fig. 8. At both displacement rates, the BTD transition, which is marked by dislocations nucleation from crack tip, occurs at $\delta = 1.5$ nm. By $\delta = 4.5$ nm, about 110 elements have been refined to full atomic resolution. We remark that this type of uniform displacement-controlled loading has been employed in many MD simulations (Rafii-Tabar et al., 2006; Rountree et al., 2002; Yu et al., 2014) and is equivalent to applying rigid grips in a tensile testing machine. The chosen boundary conditions, while not precluding crack re-direction and branching (Brommer and Buehler, 2013; Deng and Chen, 2013; Kikuchi et al., 2005), promote stable crack extension and add a constraint to the crack growth behavior such that the crack is inclined to propagate along the horizontal direction even in the presence of small perturbations like inhomogeneities or numerical errors. The double cantilever beam type of loading, which may introduce unstable crack propagation (Wetherhold and Forand, 1991), will be employed in our future work for that in this study we are more interested in exploring whether the mesh refinement theme is able to refine all elements in front of the crack tip. Because the mesh refinement criterion doesn't involve the crack propagation pathway but only considers the relative displacement between neighboring nodes which indicates the crack tip position, this mesh refinement scheme should work for the case of unstable crack extension as well.

To assess the accuracy of the adaptive mesh refinement approach, we performed MD simulations of the equivalent full atomistic models at the same displacement rates using LAMMPS (Plimpton, 1995). The same LJ potential is used. An NVE

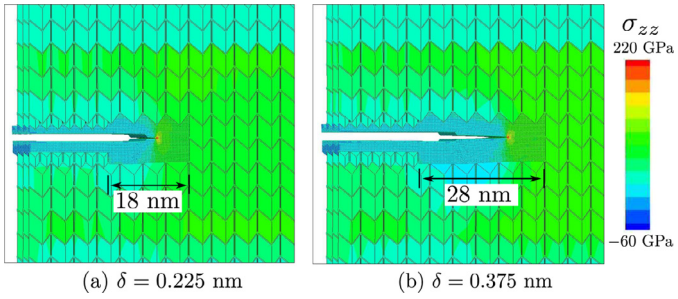

Fig. 7. The crack propagates in a brittle manner at a low strain in adaptive CAC simulations. Nodes and atoms are colored by local tensile stress σ_{zz}. At (a) $\delta =$ 0.225 nm and (b) 0.375 nm, the crack extends by 18 and 28 nm, respectively. Here, the view in Fig. 6 is rotated by about 10° around the z-axis to better image the 3-D crack. (For interpretation of the references to color in this figure legend, the reader is referred to the web version of this article.)

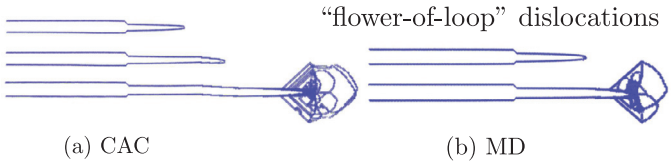

Fig. 8. Snapshots of "flower-of-loop" dislocations emitted from the crack tip during ductile fracture in both (a) CAC and (b) MD simulations. Atoms with centrosymmetry parameter (Kelchner et al., 1998) smaller than 1.3 are deleted.

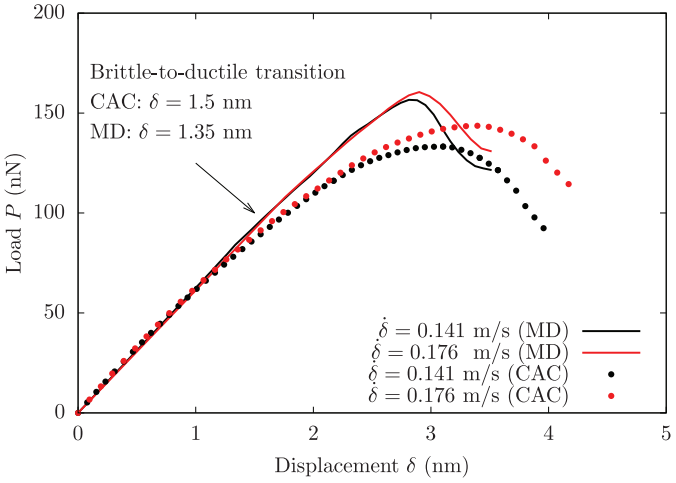

Fig. 9. Load–displacement curves of dynamic fracture at two displacement rates in both CAC and MD simulations. It is found that for both rates, the BTD transition occurs at $\delta = 1.5$ and 1.35 nm in CAC and MD simulations, respectively.

ensemble is employed with PBCs applied along the x-axis, which is consistent with the atomistic domain in CAC. In both CAC and MD, the load P is calculated by averaging the total load applied on the top and bottom layers of elements/atoms. It is found that the adaptive CAC gives similar load–displacement responses as MD and both methods show that a higher displacement rate leads to a higher specimen peak load. In MD, the BTD transition occurs at $\delta = 1.35$ nm with a smaller crack length for both displacement rates than that of CAC, as shown in Fig. 9. In addition, MD gives a slightly higher peak load than adaptive CAC, which is attributed to the reflection of waves of short wavelength at the atomistic/coarse-grained domain interface (Xiong et al., 2014a). Two separate simulations at a much lower displacement rate show that the BTD transition does not occur in either CAC or MD, i.e., the crack continues propagating throughout the whole specimen, leaving a very clean crack surface behind. A comparison of runtime between CAC and MD is not presented here because simulations are performed using different software; a detailed analysis of the coarse-graining efficiency in CAC can be found in work of Xu et al. (2015).

3.2. Curved dislocation migration

As discussed in Section 2.3, while the discontinuous elements in CAC accommodate dislocations, mesh refinement is still sometimes necessary to model dislocation migration. Consider scenarios in Fig. 4 as an example, Xiong et al. (2012a) suggest that when the slip direction of a dislocation moving from an atomistic domain is not aligned with the interelement boundaries, it can either be reflected by the atomistic/coarse-grained interface, migrate on the interface before moving into the nearest interelement boundary, or be pinned by the interface followed by nucleation of a new dislocation within the nearest interelement boundary. However, the interaction between a dislocation and domain interface at a location away from the interelement boundary was not quantified.

In this work, we performed a CAC simulation to explore the scenario where the slip plane of a mixed character curved dislocation with dominant leading screw character migrating from the atomistic domain is not aligned with the interelement boundaries in the coarse-grained domain, as shown in Fig. 10(a). The EAM potential (Daw and Baskes, 1984; Mishin et al., 2001) is employed for FCC Cu. The lattice parameter and cutoff distance are 3.615 and 5.60679 Å, respectively. The SD method with unequally-sized domains is used for parallelization. A homogeneous out-of-plane shear stress of 1 GPa is applied to drive the curved dislocation migration, with a time step of 2 fs in both domains. It is found that if the elements marked by solid green lines in Fig. 10(a) are not refined, the curved dislocation double cross-slips over the domain interface before continuing glide on a parallel slip plane, as shown in Fig. 10(b) and (c); an aphysical back stress is introduced to overcome the minimum energy barrier of Friedel–Escaig (Püschl, 2002) type double cross-slip, which is about 4 eV (Kang et al., 2014). In CAC, two mesh refinement approaches are implemented for dislocation migration: (1) a large element is manually split into two smaller ones with their boundaries along the dislocation path (Xiong et al., 2012b), and (2) the entire element is refined to atomic scale, within which the dislocation can pass smoothly; the second approach is shown in Fig. 10(d) and (e).

In Fig. 11 we compare the strain profiles between two simulations with and without mesh refinement. It is shown that the CAC simulation with mesh refinement gives a von Mises local strain invariant η^{Mises} (Shimizu et al., 2007) profile along the dislocation close to that of full atomistic simulation, while a strain concentration at the coarse-grained/atomistic domain interface occurs in the CAC simulation without mesh refinement. The strain invariant η^{Mises}, which is calculated using OVITO (Stukowski, 2010) to track the dislocation pathway in correspondence with Fig. 10, is defined by

$$\eta^{\text{Mises}} = \sqrt{E_{12}^2 + E_{13}^2 + E_{23}^2 + \frac{(E_{11}-E_{33})^2 + (E_{22}-E_{33})^2 + (E_{11}-E_{22})^2}{6}} \tag{8}$$

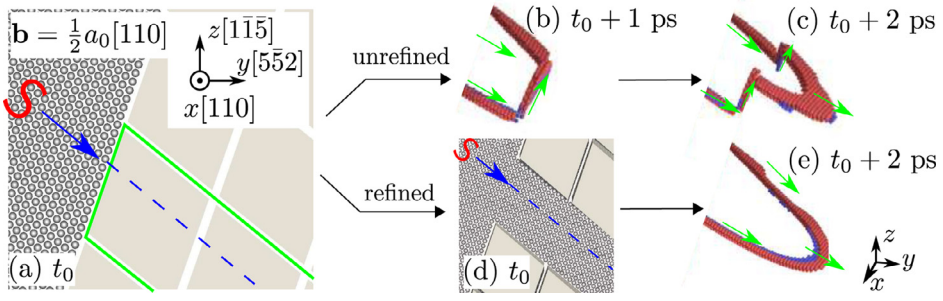

Fig. 10. (a) Illustration of the scenario where the slip plane of a curved dislocation migrating from the atomistic domain is not aligned with the interelement boundaries in the coarse-grained domain. The curved dislocation (red S) has dominant leading screw character. If the elements marked by solid green lines in (a) are not refined, the dislocation double cross-slips over the domain interface before continuing glide on a parallel slip plane, as shown in (b) and (c). (d) If the elements within solid green lines are refined to full atomistic resolution, the dislocation continues gliding on the same slip plane without cross-slip, as shown in (e). Atoms in (b), (c), and (e) are colored by adaptive common neighbor analysis (Stukowski, 2012): red are of hexagonal close packed (HCP) local structure, blue are BCC, while FCC and unrecognized atoms are deleted. A slightly different view, which is illustrated in the bottom right corner, is taken for (b), (c), and (e) to better image the double cross-slip. (For interpretation of the references to color in this figure legend, the reader is referred to the web version of this article.)

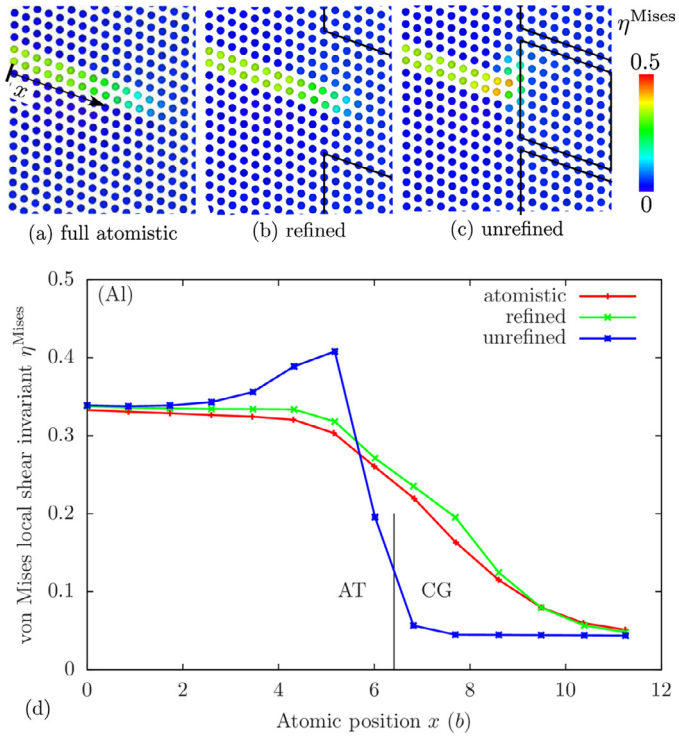

Fig. 11. The atoms are colored by von Mises local strain invariant η^{Mises} (Shimizu et al., 2007) in (a) full atomistic simulations, (b) CAC simulations with mesh refinement, and (c) CAC simulations without mesh refinement, respectively. In (d), it is found that the CAC simulation with mesh refinement gives a local strain invariant profile along the dislocation close to that of full atomistic simulation, while a strain concentration at the coarse-grained/atomistic domain interface occurs in the CAC simulation without mesh refinement. (For interpretation of the references to color in this figure legend, the reader is referred to the web version of this article.)

where E_{ij} are components of the Green–Lagrange strain tensor **E** (Zimmerman et al., 2009).

Note that the mesh refinement used for dislocation migration is performed manually here. We track the position of dislocation by analyzing the output data every 100 time steps. If some elements are to be refined, the simulation is terminated manually, before the configurations (positions and velocities of all nodes and atoms), as well as the indices of elements to be refined, are saved to restart files. Then a new simulation begins by reading the restart files and refining the marked elements following Eqs. (5) and (6). Unfortunately, a fully adaptive automated mesh refinement procedure for dislocation migration in a 3-D model remains challenging and is an ongoing work. The key to such an approach is to identify the dislocations concurrent with the simulations: in the atomistic domain, a dislocation can be detected using a dislocation extraction algorithm (Stukowski et al., 2012); in the coarse-grained domain, a nodal-based dislocation detection method can be employed to track dislocations, which will be presented in a future publication.

4. Conclusions

In this paper, two mesh refinement schemes are proposed for the CAC method, a concurrent multiscale technique. Unlike in FEM and most multiscale methods where a continuous mesh is employed, CAC accommodates dislocations between discontinuous elements. The advantage of CAC in mesh refinement includes (1) no interelement compatibility is enforced after refinement, which simplifies the procedure, (2) a minimum number of elements are refined to pass dislocations, and (3) it is straightforward to determine the positions of new atoms because the elements in CAC are assumed to correspond to actual atomic sites in lattice. These features distinguish CAC from most mesh refining multiscale methods and facilitate an efficient and straightforward implementation of mesh refinement schemes. Two parallel algorithms for CAC are discussed, which are able to re-distribute workload between processors during mesh refinement.

We first introduce an adaptive mesh refinement criterion and apply it on BTD transition in dynamic fracture of a notched specimen. Compared with MD, our adaptive CAC approach gives similar load–displacement response and local stress at crack tip, as well as an accurate prediction of the BTD transition, while eliminating most of the degrees of freedom.

We also develop a mesh refinement scheme for dislocations and apply it to a scenario where the slip plane of a curved dislocation migrating from the atomistic domain is not aligned with the interelement boundaries in the coarse-grained domain. The CAC simulation performed with mesh refinement gives a local strain invariant profile along a dislocation close to that of full atomistic simulation, while a strain concentration at the coarse-grained/atomistic domain interface occurs in the CAC simulation without mesh refinement.

With both mesh refinement schemes, the extended CAC method expands its capability to handle the evolution of more complex extended defect structures. However, this work by no means completely addresses the issues of consistency of thermodynamics between atomistic and continuum domains during adaptive mesh refinement. In the future, we will develop a fully adaptive mesh refinement scheme for dislocation migration in 3-D models. Other types of mesh refinement under consideration include, but are not limited to, *p*-refinement, *h*-refinement in which a collection of atoms are coarsened into elements, as well as an adaptive conversion between a first nearest neighbor element, which is faster but less accurate and used away from defects, and a second nearest neighbor element, which is slower but more accurate and used in the vicinity of defects (Xu et al., 2015). Attention will also be paid in constructing an *a posteriori* error estimator as well as dealing with multiple time scale issues which are potentially relevant to mesh refinement.

Acknowledgements

These results are based upon work supported by the National Science Foundation as a collaborative effort between Georgia Tech (CMMI-1232878) and University of Florida (CMMI-1233113). Any opinions, findings, and conclusions or recommendations expressed in this material are those of the authors and do not necessarily reflect the views of the National Science Foundation. The work of L.X. was supported in part by the Department of Energy, Office of Basic Energy Sciences under award no. DE-SC0006539. Q.D. also thanks support from the Fundamental Research Funds for the Central Universities (XJJ2016071), China. The authors thank Dr. Youping Chen for valuable discussions, and Mr. Rui Che for proposing and implementing the adaptive mesh refinement scheme in CAC and for carrying out the dynamic fracture simulations. This work used the Extreme Science and Engineering Discovery Environment (XSEDE), which is supported by National Science Foundation grant number ACI-1053575.

References

Abraham, F.F., 1997. On the transition from brittle to plastic failure in breaking a nanocrystal under tension (NUT). Europhys. Lett. 38 (2), 103–106.
Abraham, F.F., Broughton, J.Q., Bernstein, N., Kaxiras, E., 1998. Spanning the continuum to quantum length scales in a dynamic simulation of brittle fracture. Europhys. Lett. 44 (6), 783–787.
Abraham, F.F., Schneider, D., Land, B., Lifka, D., Skovira, J., Gerner, J., Rosenkrantz, M., 1997. Instability dynamics in three-dimensional fracture: An atomistic simulation. J. Mech. Phys. Solids 45 (9), 1461–1471.

Arndt, M., Luskin, M., 2008. Goal-oriented adaptive mesh refinement for the quasicontinuum approximation of a Frenkel–Kontorova model. Comput. Meth. Appl. Mech. Eng. 197 (49–50), 4298–4306.

Belytschko, T., Black, T., 1999. Elastic crack growth in finite elements with minimal remeshing. Int. J. Numer. Meth. Eng. 45 (5), 601–620.

Belytschko, T., Liu, W.K., Moran, B., Elkhodary, K., 2014. Nonlinear Finite Elements for Continua and Structures, second Wiley, Chichester, West Sussex, UK.

Belytschko, T., Mos, N., Usui, S., Parimi, C., 2001. Arbitrary discontinuities in finite elements. Int. J. Numer. Meth. Eng. 50 (4), 993–1013.

Bitzek, E., Kermode, J.R., Gumbsch, P., 2015. Atomistic aspects of fracture. Int. J. Fract. 191 (1-2), 13–30.

Brommer, D.B., Buehler, M.J., 2013. Failure of graphdiyne: structurally directed delocalized crack propagation. J. Appl. Mech. 80 (4), 040908.

Brünger, A., Brooks III, C.L., Karplus, M., 1984. Stochastic boundary conditions for molecular dynamics simulations of ST2 water. Chem. Phys. Lett. 105 (5), 495–500.

Chapra, S., Canale, R., 2009. Numerical Methods for Engineers, sixth McGraw-Hill Science/Engineering/Math, Boston.

Chen, Y., 2006. Local stress and heat flux in atomistic systems involving three-body forces. J. Chem. Phys. 124 (5), 054113.

Chen, Y., 2009. Reformulation of microscopic balance equations for multiscale materials modeling. J. Chem. Phys. 130 (13), 134706.

Chen, Y., Lee, J., 2005. Atomistic formulation of a multiscale field theory for nano/micro solids. Phil. Mag. 85 (33–35), 4095–4126.

Chen, Y., Lee, J.D., 2003. Connecting molecular dynamics to micromorphic theory. (I). Instantaneous and averaged mechanical variables. Phys. A: Stat. Mech. Appl. 322, 359–376.

Chen, Y., Lee, J.D., 2003. Connecting molecular dynamics to micromorphic theory. (II). Balance laws. Phys. A: Stat. Mech. Appl. 322, 377–392.

Chen, Y., Lee, J.D., 2003. Determining material constants in micromorphic theory through phonon dispersion relations. Int. J. Eng. Sci. 41 (8), 871–886.

Chen, Y., Zimmerman, J., Krivtsov, A., McDowell, D.L., 2011. Assessment of atomistic coarse-graining methods. Int. J. Eng. Sci. 49 (12), 1337–1349.

Cheung, K.S., Yip, S., 1994. A molecular-dynamics simulation of crack-tip extension: The brittle-to-ductile transition. Model. Simul. Mater. Sci. Eng. 2 (4), 865–892.

Daw, M.S., Baskes, M.I., 1984. Embedded-atom method: Derivation and application to impurities, surfaces, and other defects in metals. Phys. Rev. B 29 (12), 6443–6453.

Deng, Q., Chen, Y., 2013. A coarse-grained atomistic method for 3d dynamic fracture simulation. Int. J. Multiscale Comput. Eng. 11 (3), 227–237.

Deng, Q., Xiong, L., Chen, Y., 2010. Coarse-graining atomistic dynamics of brittle fracture by finite element method. Int. J. Plast. 26 (9), 1402–1414.

Gracie, R., Belytschko, T., 2009. Concurrently coupled atomistic and XFEM models for dislocations and cracks. Int. J. Numer. Meth. Eng. 78 (3), 354–378.

Gracie, R., Belytschko, T., 2011. An adaptive concurrent multiscale method for the dynamic simulation of dislocations. Int. J. Numer. Meth. Eng. 86 (4–5), 575–597.

Gumbsch, P., Riedle, J., Hartmaier, A., Fischmeister, H.F., 1998. Controlling factors for the brittle-to-ductile transition in tungsten single crystals. Science 282 (5392), 1293–1295.

Kang, K., Yin, J., Cai, W., 2014. Stress dependence of cross slip energy barrier for face-centered cubic nickel. J. Mech. Phys. Solids 62, 181–193.

Kelchner, C.L., Plimpton, S.J., Hamilton, J.C., 1998. Dislocation nucleation and defect structure during surface indentation. Phys. Rev. B 58 (17), 11085–11088.

Kikuchi, H., Kalia, R.K., Nakano, A., Vashishta, P., Branicio, P.S., Shimojo, F., 2005. Brittle dynamic fracture of crystalline cubic silicon carbide (3C-SiC) via molecular dynamics simulation. J. Appl. Phys. 98 (10), 103524.

Kluge, M.D., Wolf, D., Lutsko, J.F., Phillpot, S.R., 1990. Formalism for the calculation of local elastic constants at grain boundaries by means of atomistic simulation. J. Appl. Phys. 67 (5), 2370–2379.

Kwon, S., Lee, Y., Park, J.Y., Sohn, D., Lim, J.H., Im, S., 2009. An efficient three-dimensional adaptive quasicontinuum method using variable-node elements. J. Comput. Phys. 228 (13), 4789–4810.

Miller, R.E., Tadmor, E.B., 2002. The Quasicontinuum method: Overview, applications and current directions. J. Comput.-Aid. Mater. Des. 9 (3), 203–239.

Mishin, Y., Mehl, M.J., Papaconstantopoulos, D.A., Voter, A.F., Kress, J.D., 2001. Structural stability and lattice defects in copper: Ab initio, tight-binding, and embedded-atom calculations. Phys. Rev. B 63 (22), 224106.

Moës, N., Dolbow, J., Belytschko, T., 1999. A finite element method for crack growth without remeshing. Int. J. Numer. Meth. Eng. 46 (1), 131–150.

Moseley, P., Oswald, J., Belytschko, T., 2012. Adaptive atomistic-to-continuum modeling of propagating defects. Int. J. Numer. Meth. Eng. 92 (10), 835–856.

Park, J.Y., Im, S., 2008. Adaptive nonlocal quasicontinuum for deformations of curved crystalline structures. Phys. Rev. B 77 (18), 184109.

Pavia, F., Curtin, W.A., 2015. Parallel algorithm for multiscale atomistic/continuum simulations using LAMMPS. Model. Simul. Mater. Sci. Eng. 23 (5), 055002.

Plimpton, S., 1995. Fast parallel algorithms for short-range molecular dynamics. J. Comput. Phys. 117 (1), 1–19.

Püschl, W., 2002. Models for dislocation cross-slip in close-packed crystal structures: a critical review. Prog. Mater. Sci. 47 (4), 415–461.

Rafii-Tabar, H., Shodja, H.M., Darabi, M., Dahi, A., 2006. Molecular dynamics simulation of crack propagation in fcc materials containing clusters of impurities. Mech. Mater. 38 (3), 243–252.

Rountree, C.L., Kalia, R.K., Lidorikis, E., Nakano, A., Van Brutzel, L., Vashishta, P., 2002. Atomistic aspects of crack propagation in brittle materials: Multimillion atom molecular dynamics simulations. Annu. Rev. Mater. Res. 32 (1), 377–400.

Rudd, R., Broughton, J., 2000. Concurrent coupling of length scales in solid state systems. Phys. Status Solid. (b) 217 (1), 251–291.

Schroeder, W., Martin, K., Lorensen, B., 2006. Visualization Toolkit: An Object-Oriented Approach to 3D Graphics, 4th Kitware.

Schulson, E.M., Barker, D.R., 1983. A brittle to ductile transition in NiAl of a critical grain size. Scripta Metall. 17 (4), 519–522.

Shenoy, V., Shenoy, V., Phillips, R., 1998. Finite temperature quasicontinuum methods. In: Symposium: Multiscale Modelling Material. In: MRS Online Proceedings Library, vol. 538, pp. 465–471.

Shilkrot, L., Miller, R.E., Curtin, W.A., 2004. Multiscale plasticity modeling: coupled atomistics and discrete dislocation mechanics. J. Mech. Phys. Solids 52 (4), 755–787.

Shimizu, F., Ogata, S., Li, J., 2007. Theory of shear banding in metallic glasses and molecular dynamics calculations. Mater. Trans. 48 (11), 2923–2927.

Stukowski, A., 2010. Visualization and analysis of atomistic simulation data with OVITO—the Open Visualization Tool. Model. Simul. Mater. Sci. Eng. 18 (1), 015012.

Stukowski, A., 2012. Structure identification methods for atomistic simulations of crystalline materials. Modelling Simul. Mater. Sci. Eng. 20 (4), 045021.

Stukowski, A., Bulatov, V.V., Arsenlis, A., 2012. Automated identification and indexing of dislocations in crystal interfaces. Model. Simul. Mater. Sci. Eng. 20 (8), 085007.

Tadmor, E.B., Miller, R., 2012. Modeling Materials: Continuum, Atomistic and Multiscale Techniques. Cambridge University Press.

Tadmor, E.B., Ortiz, M., Phillips, R., 1996. Quasicontinuum analysis of defects in solids. Philos. Mag. A 73 (6), 1529–1563.

Towns, J., Cockerill, T., Dahan, M., Foster, I., Gaither, K., Grimshaw, A., Hazlewood, V., Lathrop, S., Lifka, D., Peterson, G., Roskies, R., Scott, J., Wilkins-Diehr, N., 2014. XSEDE: Accelerating scientific discovery. Comput. Sci. Eng. 16 (5), 62–74.

Verlet, L., 1967. Computer “experiments” on classical fluids. I. Thermodynamical properties of Lennard-Jones molecules. Phys. Rev. 159 (1), 98–103.

Wetherhold, R.C., Forand, J.A., 1991. Improving stability in the double-cantilever-beam fracture test. Mater. Sci. Eng.: A 147 (1), L17–L20.

Xiong, L., Chen, X., Zhang, N., McDowell, D.L., Chen, Y., 2014. Prediction of phonon properties of 1d polyatomic systems using concurrent atomisticcontinuum simulation. Arch. Appl. Mech. 84 (9–11), 1665–1675.

Xiong, L., Chen, Y., 2009. Multiscale modeling and simulation of single-crystal MgO through an atomistic field theory. Int. J. Solids Struct. 46 (6), 1448–1455.

Xiong, L., Chen, Y., 2012. Coarse-grained atomistic modeling and simulation of inelastic material behavior. Acta Mech. Solida Sinica 25 (3), 244–261.

Xiong, L., Deng, Q., Tucker, G., McDowell, D.L., Chen, Y., 2012. A concurrent scheme for passing dislocations from atomistic to continuum domains. Acta Mater. 60 (3), 899–913.

Xiong, L., Deng, Q., Tucker, G.J., McDowell, D.L., Chen, Y., 2012. Coarse-grained atomistic simulations of dislocations in Al, Ni and Cu crystals. Int. J. Plast. 38, 86–101.

Xiong, L., McDowell, D.L., Chen, Y., 2014. Sub-THz Phonon drag on dislocations by coarse-grained atomistic simulations. Int. J. Plast. 55, 268–278.

Xiong, L., Rigelesaiyin, J., Chen, X., Xu, S., McDowell, D.L., Chen, Y., 2016. Coarse–grained elastodynamics of fast moving dislocations. Acta Mater. 104, 143–155.

Xiong, L., Tucker, G., McDowell, D.L., Chen, Y., 2011. Coarse-grained atomistic simulation of dislocations. J. Mech. Phys. Solids 59 (2), 160–177.

Xu, G., 2005. Dislocation nucleation from crack tips and brittle to ductile transitions in cleavage fracture. In: Hirth, J., Nabarro, F. (Eds.), Dislocations in Solids, vol. 12. Elsevier, pp. 81–145.

Xu, S., Che, R., Xiong, L., Chen, Y., McDowell, D.L., 2015. A quasistatic implementation of the concurrent atomistic-continuum method for FCC crystals. Int. J. Plast. 72, 91–126.

Xu, S., Xiong, L., Chen, Y., McDowell, D.L., 2016. Sequential slip transfer of mixed-character dislocations across $\Sigma 3$ coherent twin boundary in FCC metals: a concurrent atomistic-continuum study. Comput. Mater. 2, 15016.

Yu, J., Zhang, Q., Liu, R., Yue, Z., Tang, M., Li, X., 2014. Molecular dynamics simulation of crack propagation behaviors at the Ni/Ni_3Al grain boundary. RSC Adv. 4 (62), 32749–32754.

Zienkiewicz, O.C., Taylor, R.L., Zhu, J.Z., 2013. The Finite Element Method: Its Basis and Fundamentals, seventh Butterworth-Heinemann, Amsterdam.

Zimmerman, J.A., Bammann, D.J., Gao, H., 2009. Deformation gradients for continuum mechanical analysis of atomistic simulations. Int. J. Solids Struct. 46 (2), 238–253.